

***Ab initio* calculations of the concentration dependent band gap reduction in dilute nitrides**Phil Rosenow,<sup>1</sup> Lars C. Bannow,<sup>2</sup> Eric W. Fischer,<sup>1</sup> Wolfgang Stolz,<sup>3</sup> Kerstin Volz,<sup>2,3</sup> Stephan W. Koch,<sup>2,3</sup> and Ralf Tonner<sup>1,3,\*</sup><sup>1</sup>*Fachbereich Chemie, Philipps-Universität Marburg, Hans-Meerwein-Straße 4, 35032 Marburg, Germany*<sup>2</sup>*Fachbereich Physik, Philipps-Universität Marburg, Renthof 5, 35032 Marburg, Germany*<sup>3</sup>*Material Sciences Center, Philipps-Universität Marburg, Hans-Meerwein-Straße 6, 35032 Marburg, Germany*

(Received 8 June 2017; revised manuscript received 15 January 2018; published 1 February 2018)

While being of persistent interest for the integration of lattice-matched laser devices with silicon circuits, the electronic structure of dilute nitride III/V-semiconductors has presented a challenge to *ab initio* computational approaches. The origin of the computational problems is the strong distortion exerted by the N atoms on most host materials. Here, these issues are resolved by combining density functional theory calculations based on the meta-GGA functional presented by Tran and Blaha (TB09) with a supercell approach for the dilute nitride Ga(NAs). Exploring the requirements posed to supercells, it is shown that the distortion field of a single N atom must be allowed to decrease so far that it does not overlap with its periodic images. This also prevents spurious electronic interactions between translational symmetric atoms, allowing us to compute band gaps in very good agreement with experimentally derived reference values. In addition to existing approaches, these results offer a promising *ab initio* avenue to the electronic structure of dilute nitride semiconductor compounds.

DOI: [10.1103/PhysRevB.97.075201](https://doi.org/10.1103/PhysRevB.97.075201)**I. INTRODUCTION**

In recent years, semiconductor compounds based on gallium arsenide (GaAs) containing small amounts of nitrogen (N) have proven to be promising materials for a wide range of optoelectronic applications such as (GaIn)(NAs) laser diodes [1]. More recently, silicon-matched Ga(NAsP) structures as laser active materials have become a highly active area of research [2]. Since the band gap of GaN was known to be larger than that of GaAs, a blueshift of the photoluminescence (PL) edge was expected for Ga(NAs). However, the first experimental PL of dilute nitride Ga(NAs) measured by Weyers *et al.* [3] showed a redshift of the PL. Further studies showed that the underlying band gap bowing was unusually strong [4,5].

In contrast to other III/V semiconductors, the description of bowing within the commonly used virtual crystal approximation agrees less well with experimental band gaps than the slightly more involved conduction band anticrossing (CBAC) model [6,7]. Unlike the related material Ga(NP), where the nitrogen states lie within the band gap at small concentrations [8], states arising from isolated and clustered nitrogen atoms in Ga(NAs) occur above the conduction band edge. While this strong concentration dependence allows us to specifically manipulate the band gap by controlling the composition, the unexpected strength of this effect also called for an explanation.

Based on density functional theory (DFT) and quasiparticle (GW) calculations, Rubio and Cohen [9] were able to attribute the N concentration dependent changes to an increase of the volume caused by the lattice mismatch, lowering the energy of the conduction band (CB) edge, which is strongly localized on the N atoms. Further studies, mainly based on DFT within the local density approximation (LDA), were performed in the following years [10–13]. A study based on the hybrid functional

HSE06 showed an improved agreement with the observed band gap bowing [14]. Regarding the origin of the strong bowing, further studies found that the CB states centered on the N atoms are extended especially along the zigzag lines in the zinc blende structure [15,16].

In the context of our work, it is noteworthy that none of the cited *ab initio* results reproduced the band gaps accurately. To correct this, Zunger *et al.* constructed empirical pseudopotentials fitted to GW band structures, experimentally determined band gaps, and LDA deformation potentials. This allowed them to perform calculations with huge supercells (13 824 atoms) [11,12,15]. Thereby, they showed that the large lattice mismatch between As and N leads to long range strain fields [15]. This, and the extension of N-centered CB states, indicates the need for large supercells [17].

For the quantitative modeling and development of dilute nitride based optoelectronic devices, it is desirable to predict the optical properties of these materials. This requires an accurate *ab initio* description of the band structure and the band gap without using empirical or experimental parameters. While DFT is most often the method of choice in material science, there are two factors that usually prevent a quantitative description using DFT supercell calculations: Firstly, commonly used density functionals mostly underestimate the band gap of semiconductors considerably (LDA [18,19], PBE [20]). Hybrid functionals including exact exchange like HSE06 [21] (more recently used with tailored parameters [22]) can solve this issue but are computationally more demanding and hardly applicable to supercells with several hundred atoms in a routine fashion. Secondly, the enormous lattice mismatch between GaN and GaAs due to the size difference of As and N (the lattice constant of GaN is roughly 80% that of GaAs) in combination with the periodicity of the finite size supercells cause an artificial reduction of the band gap [15,16]. Overcoming the latter problem requires large supercells which adds to the former by increasing the computational cost. An

\*tonner@chemie.uni-marburg.de

alternative approach is to use special quasirandom structures (SQS) as proposed by Zunger *et al.*, which aim to emulate a random distribution in a semiconductor alloy [23]. This approach has often been successfully used in the past but requires convergence with respect to cell size nonetheless. Therefore, a functional capable of accurately describing the band gap while still being computationally efficient is needed.

The recently developed meta-GGA functional TB09 (also known as mBJLDA or TB-mBJ) [24] is a promising candidate to fulfill these requirements for Ga(NAs). It has been shown that TB09 allows the user to obtain band gaps commonly in good agreement with experimental data [24–26] while being computationally very efficient in comparison to HSE06 and GW calculations [24].

In this paper, we will use the TB09 functional in combination with fairly large supercells (up to 432 atoms) to solve the long standing issue of the *ab initio* prediction of accurate band gaps in dilute nitrides. In Sec. II, we introduce our computational methods and parameters. Thereafter, we present our results, starting with a brief validation of the approach used followed by a discussion of the structural effects of nitrogen incorporation and finally the effect on the band gap for different supercells.

## II. COMPUTATIONAL METHOD

DFT calculations were performed using the Vienna *ab initio* simulation package (VASP 5.3.5) [27–30] with a plane wave basis in conjunction with the projector-augmented wave method [31,32]. The basis set energy cutoff was set to 450 eV for optimizations and 350 eV for large supercell band gap computations. The reciprocal space was sampled with a  $\Gamma$ -centered Monkhorst-Pack grid with six intersections per direction for primitive unit cells and an accordingly reduced set for supercells [33]. Cell relaxations of primitive cells and all lattice relaxations were done with the PBE functional [20], corrected for dispersion interactions with the DFT-D3 scheme [34,35]. Lattice parameters for binary materials were derived from fitting the Vinet equation of state, yielding a theoretically optimized value [36]. The lattice parameters for ternary cells were linearly interpolated from the constituents (Vegard’s rule). For  $6^3$  supercells with more than one N atom, sampling was performed by randomly selecting As atoms to be replaced by N atoms and averaging over few arrangements. For a small number of N atoms, more qualitatively distinct arrangements (e.g., different average distances) are possible; thus, more arrangements were sampled for smaller concentrations. Calculations of band gaps and band structures used the TB09 functional [24] as well as PBE0 [37], HSE06 [21], and LDA-1/2 [38,39] functionals for comparison. Potentials for the LDA-1/2 calculations were prepared using the ATOM code with a cutoff (in a.u.) of 0.9875 for Ga, 3.7725 for As, 3.6550 for P, and 2.9275 for N [38,40]. In addition,  $G_0W_0$  calculations were carried out based on the PBE orbitals. For all band gap computations, spin-orbit coupling was considered, with the exception of  $G_0W_0$ . For relaxations, the electronic energy and forces were converged to  $10^{-6}$  eV and  $10^{-2}$  eV  $\text{\AA}^{-1}$ , respectively. The electronic energy and eigenvalues for band gap computations in supercells were converged to  $10^{-4}$  eV.

TABLE I. Direct band gap (eV) of III/V semiconductors in zinc blende structure with various methods.  $G_0W_0$  is based on PBE and without spin-orbit coupling. Lattice constants (GaAs: 5.689  $\text{\AA}$ , GaN: 4.580  $\text{\AA}$ , GaP: 5.477  $\text{\AA}$ ) were theoretically optimized (PBE-D3) as described in the method section. The root mean square deviation (RMSD) w.r.t. experimental reference values is given for each method.

	PBE	LDA-1/2	PBE0	HSE06	TB09	$G_0W_0$ (PBE)	Ref. [44]
GaAs	0.32	1.17	1.71	1.11	1.44	1.41	1.52
GaN	1.58	3.16	3.48	2.78	3.03	3.09	3.28
GaP	1.74	2.58	3.31	2.66	2.95	2.86	2.86
RMSD	1.36	0.27	0.30	0.39	0.16	0.13	

A supercell calculation yields an energy dispersion  $E(\mathbf{K})$  where  $\mathbf{K}$  is the wave vector in the reciprocal space of the supercell. Often, it is desirable to project the supercell eigenstates  $|\mathbf{K}, n\rangle$  on the eigenstates  $|\mathbf{k}_j, m\rangle$  of the respective primitive cell. The index  $j$  accounts for the fact that every supercell eigenstate matches  $N^3$  primitive cell eigenstates where  $N$  depends on the size of the supercell. Thus, a so-called *effective* band structure (EBS)  $E(\mathbf{k})$  can be extracted. For this, we calculate the spectral weight that is a measure for the Bloch character of a specific eigenstate. We follow the steps outlined in the appendix of Ref. [41]. The spectral weight  $w_{n,\mathbf{k}}(\mathbf{k})$  is given by the square sum of the relevant plane wave coefficients

$$w_{n,\mathbf{k}}(\mathbf{k}_j) = \sum_{\mathbf{g}} |C_{n,\mathbf{k}}(\mathbf{g} + \mathbf{G}_j)|^2, \quad (1)$$

where  $n$  is the band index and  $\mathbf{g}$  and  $\mathbf{G}_j$  are reciprocal lattice vectors of the primitive cell and the supercell, respectively.

Apart from cubic supercells, SQS cells have been used for ternary compounds [23]. SQS cells have been generated with the alloy-theoretic automated toolkit (ATAT) [42], with correlations between two atoms up to the third sphere of the same lattice site, three atoms up to the second sphere and four atoms in the first sphere only, corresponding to four distinct two-atom clusters, ten three-atom clusters, and two four-atom clusters.

The  $(N \times N \times N)$  supercells of the primitive zinc blende unit cell will be referred to as  $N^3$  supercells, SQS cells with  $N$  atoms as SQS- $N$ . Structures and band gaps for the used cells are shown in the Supplemental Material [43].

## III. NUMERICAL RESULTS AND ANALYSIS

### A. Method benchmark

First, we revisit the question of band gap computation for common functional classes. Table I shows a comparison of band gaps from PBE, LDA-1/2, PBE0, HSE06, and TB09 together with the quasiparticle approach  $G_0W_0$  for binary III/V semiconductors GaAs, GaN, and GaP at theoretically optimized lattice constants. While PBE shows the well-known shortcoming of GGA functionals for band gap computations, the LDA-1/2 approach and the hybrid functionals achieve a decent agreement both with the many-body approach and experimental values. However, the TB09 functional clearly outperforms the other density functionals in terms of accuracy

TABLE II. Displacement relative to ideal lattice site of selected atoms in  $\text{Ga}_{125}(\text{As}_{124}\text{N}_1)$  compared to  $\text{Ga}_{125}(\text{As}_{124}\text{Bi}_1)$  in Å. Labeling of position relative to atom  $E$  and according to Fig. 1.

	$\text{Ga}_{125}(\text{As}_{124}\text{N}_1)$	$\text{Ga}_{125}(\text{As}_{124}\text{Bi}_1)$
$\text{Ga}_{\text{NN}}$	-0.379	0.190
$\text{As}_{\text{NNN}}$	-0.110	0.053
$\text{Ga}_{3\text{N}}(\text{on})$	-0.067	0.036
$\text{Ga}_{3\text{N}}(\text{off})$	-0.017	0.008
$\text{As}_{4\text{N}}(\text{on})$	-0.032	0.019
$\text{Ga}_{5\text{N}}(\text{on})$	-0.005	0.003

and competes very well with the much more demanding GW method, indicating its suitability for the band gap calculation of large supercells. In terms of computational effort, TB09 is slightly more demanding than GGA functionals but less than hybrid functionals or the GW method. Thus, we selected this functional to compute the electronic structure of the compounds.

### B. Structural effect of N incorporation compared to other group V elements

It has been shown before that from the available group V atoms in the GaAs lattice, incorporation of N results in the by far strongest displacement of nearest neighbor Ga atoms. The N incorporation leads to roughly twice the displacement from ideal lattice position (-0.379 Å) compared to the other extreme in that group, Bi (+0.190 Å). This lattice distortion enhances the extension of the nitrogen state in real space, causing the interaction with translational images of the atom. This is the underlying cause for the artificial band gap reduction described above. Beyond nearest neighbors, the distortion propagates further and is highly anisotropic. We show this for a  $5^3$  supercell with one As atom replaced by N and Bi, respectively. Both cells have the lattice constant of the respective compound and the atomic positions have been relaxed. The distortion is shown in Table II in terms of displacement for an atom at a given position relative to atom  $E$  ( $E = \text{N}, \text{Bi}$ ). The labeling of these positions is explained in Fig. 1 and is based on the connectivity to atom  $E$  along chemical bonds rather than spatial distance. For the first two coordination spheres, i.e., the nearest neighbors (NN) and next-nearest neighbors (NNN), the distortion is isotropic. At the third-nearest neighbors (3N) positions, a distinction can be made between the Ga atoms along the  $\{110\}$  zigzag chains [ $\text{Ga}_{3\text{N}}(\text{on})$ ] and those sitting off these chains [ $\text{Ga}_{3\text{N}}(\text{off})$ ]. While the former are further away from atoms  $E$  in terms of spatial

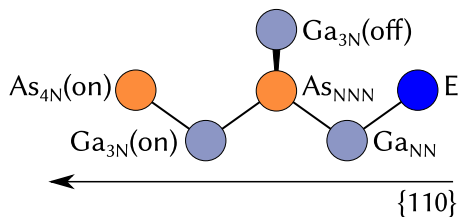


FIG. 1. Schematic representation of the environment of an atom  $E$  in GaAs lattice with  $E = \text{N}, \text{Bi}$ .

TABLE III. Band gaps of the  $3^3$  and one  $6^3$  supercells with 3.7% N for the unrelaxed and relaxed structure and the relaxed structure, where N has been replaced with As. All values in eV.

Supercell	GaAs	$\text{GaAs}(d_{\text{Ga}(\text{NAs})})$	unrelaxed	relaxed	As-for-N
$3^3$	1.44	1.61	1.19	0.58	1.39
$6^3$			1.39	1.06	1.51

distance than the latter, their displacement is about four times as large. Along the  $\{110\}$  directions, every step beyond the next-nearest-neighbor spheres approximately halves the distortion. Comparing Ga(NAs) and Ga(AsBi), the distance over which the GaAs lattice surrounding atom  $E$  is relaxed is twice as large for the dilute nitride as for the bismide, in accordance with their difference in atomic radius. This explains, why dilute bismides can be described well with moderately sized supercells [7] in contrast to dilute nitrides.

Since the displacement is halved with every step to the next position, it should decay to sub-pm magnitude with the 6N position in the labeling used here. In the  $5^3$  supercell, the 5N position is already halfway between the N atom and its periodic image and is as such balanced by those (the displacement is perpendicular to the connection between the N atom and its periodic image and a result of the displacement of neighboring atoms). By extrapolation to the next largest cell size, the strain field can be expected to be sufficiently decayed.

In general terms, a supercell must allow for the strain to decay far enough that the strain fields of translational images do not interfere in an artificial way. For the concentration range used in this paper, the strain decay data suggests that a  $6^3$  supercell is sufficient. For larger concentrations or specific clustered arrangements, larger supercells may be necessary.

### C. Band gap evolution for small and large supercells

In order to study the effect of the cell size on the band gap of a dilute nitride, it is instructive to compare properties of two cubic supercells with the same N concentration. Thus, two supercells of different size for 3.7% N have been taken to study different contributions to the band gap reduction due to N incorporation. The smaller one is a  $3^3$  supercell (54 atoms in total, one N), the larger one a  $6^3$  supercell (432 atoms in total, eight N). For the larger supercell, four different random arrangements of the N atoms have been sampled (see Sec. II). One of these showed excellent agreement with the CBAC reference and will be used as an example in the remainder of this paragraph [see Fig. 2(b) for the structure]. Following Kent and Zunger [15], different contributions to the band gap change can be distinguished. In the first step, the lattice constant of GaAs is changed to that of the Ga(NAs) compound, which increases the band gap to 1.61 eV, see Table III. An appropriate number of As atoms in each cell is replaced by N atoms in the second step, without relaxing the structure. This changes the band gap by different amounts for each supercell size: by -0.42 eV for the  $3^3$  supercell and by -0.22 eV for the  $6^3$  supercell, showing the smaller finite size effect for the latter. In the third step, the lattice positions are relaxed, further reducing the band gap to 0.58 eV for the  $3^3$  and to 1.06 eV for the  $6^3$

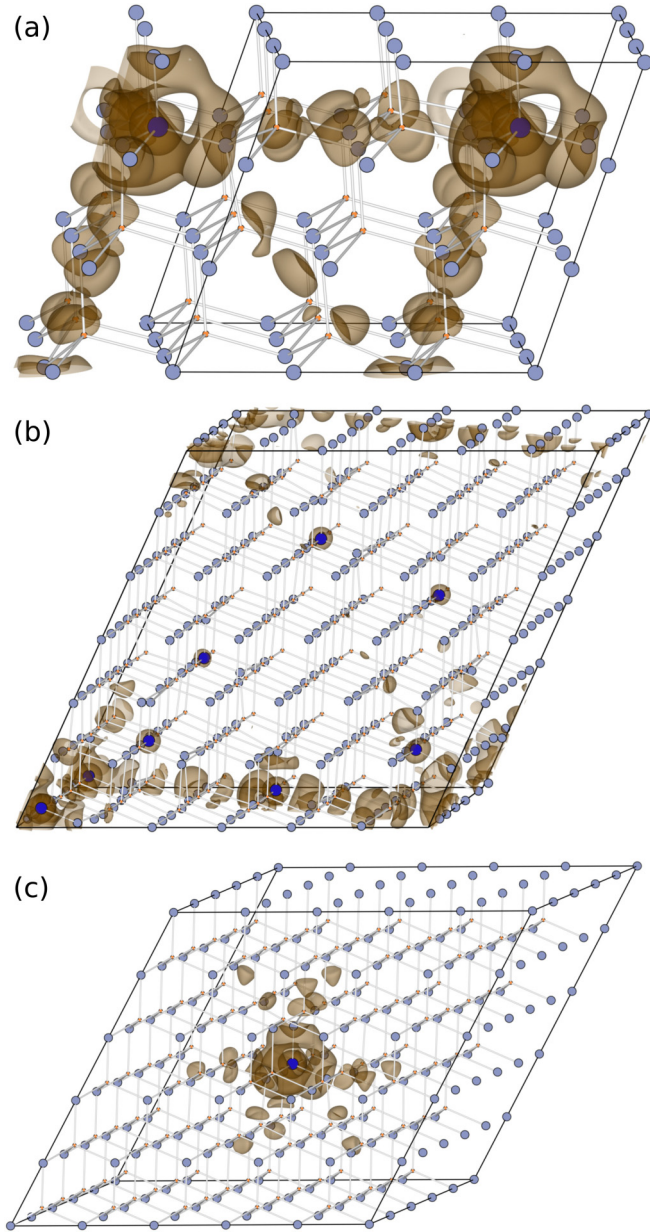


FIG. 2. Partial charge density of the first conduction band of Ga(NAs) with 3.7% N (a)  $3^3$  supercell, (b)  $6^3$  supercell and 0.8% N, (c)  $5^3$  supercell. Isosurface at 10% of the respective maximal value. Ga: light blue, As: orange, N: blue; Ga and As atoms are shown in smaller size.

supercell. Especially this last step clearly shows the spurious interactions of translational images in small supercells.

Finally, it is instructive to replace the N atoms in the relaxed structure again by As atoms in order to separate electronic and structural effects. In this case, the band gap of the  $3^3$  supercell is 0.12 eV smaller than that of the  $6^3$  supercell which emphasizes the dampened effect of the strain field in the latter. It should be stressed that the electronic and structural contributions are not additive and synergy between both effects can be observed.

The relaxation step in our procedure can be further divided in two different ways. First, following the band gap along the relaxation by computing it for partly relaxed structures, it can be seen that the band gap reduction is linear with relaxation,

TABLE IV. Band gaps of Ga(NAs) with various N concentrations and supercell types and sizes. Cubic  $3^3$  and  $6^3$  supercells as well as SQS-54, -108, -162, and -216 cells have been used for N concentrations of 3.7, 7.4, and 11.1%. Values were obtained by averaging over several arrangements for the  $N^3$  supercells with the exception of the  $3^3$  cell for 3.7%, for which only one arrangement exists. Direct band gaps in eV.

% N	$3^3$	$6^3$	S-54	S-108	S-162	S-216	Ref. [45]
3.7	0.58	1.00	0.91	0.99	1.30	1.17	1.06
7.4	0.31	0.77	0.87	0.92	0.93	0.86	0.85
11.1	0.20	0.63	0.25	0.35	0.28	0.24	0.68
RMSD	0.50	0.06	0.26	0.20	0.27	0.26	

showing a simple relationship between structural deformation and change in the band gap. This emphasizes the bigger effect on the band gap when combining strongly mismatched materials. Secondly, relaxing only the four nearest neighbors of the N atom accounts for 97% of the band gap reduction, showing that the overlap between N and nearest neighbor Ga atoms is most influential for the stabilization of the states at the CB edge.

#### D. Extension of N states in real space

The partial charge densities of the first conduction band of both cells discussed in the previous section are shown in Fig. 2. As was already described previously [15], for the too small  $3^3$  supercell the N atom interacts with its own translational image [Fig. 2(a)]. Also, the charge density spreads along the {110}-zigzag chains. In the case of the larger  $6^3$  supercell, the partial charge density is spread mainly over three N atoms and the chains in between those [Fig. 2(b)]. While some artificial periodicity clearly remains, there is no such spurious interaction between translational images as for the smaller cell. For an unrelaxed lattice, the N state is localized at the N atom itself, without spreading through the lattice (not shown). Thus, the strong combined relaxation effect for too small supercells described above is well reflected in the real space electronic structure. The corresponding partial charge density for the  $5^3$  supercell used to study structural effects is shown as well [Fig. 2(c)]. It is sufficiently localized at the N atom and contained within the unit cell to avoid artificial interaction over the cell boundaries. These observations agree well with the structural finding above, since the CB states are extended mainly along the same zigzag lines, on which the strain field propagates. In a real space picture, the reduced interatomic distance along these lines increases the orbital overlap, thereby increasing the extension of the N-centered state.

#### E. Band gaps of dilute nitrides for concentrations up to 11%

While the  $6^3$  supercell clearly is better suited than the smaller  $3^3$  supercell, it remains to be determined if it is large enough to reproduce accurate band gaps for nitrides over a relevant concentration range. To this end, both simple supercells and SQS cells of increasing size are compared for various concentrations with reference values from an established CBAC [45] model in Table IV. It should be stated

that the CBAC parameters are based on measured band gaps for concentrations up to 5% only. Given the lack of available data for higher concentrations, an extrapolation of the CBAC model to concentrations of interest to this work was applied to be used as a reference. In addition, tight-binding calculations suggest a smooth band gap dependence on the concentration in this range [46]. For all concentrations, the  $3^3$  supercells perform not only considerably worse than the  $6^3$  cells, but show deficits for increasing concentrations of N, especially for specific arrangements of atoms in the cell (a particular arrangement of three N atoms bound to one Ga atom almost closes the band gap for 11.1% N). An average deviation from the reference of  $-0.50$  eV demonstrates the effect of the spurious interaction between electronic states of periodic images of N atoms for the  $3^3$  supercells. The larger supercells on the other side agree with the reference values within the accuracy that can be expected from the functional, on average underestimating the reference by approximately 0.06 eV, and are thus large enough to overcome the artificial band gap reduction caused by the periodic boundary conditions. This shows that the combination of an accurate yet feasible functional with moderately large unit cells allows quantitative, predictive computations of dilute nitride band gaps.

Furthermore, SQS cells were investigated regarding their suitability for predictive band gap computations. This approach is designed to efficiently model random structures with periodic boundary conditions. As such it saves the need for sampling and generally reduces the required cell size. Given the notorious difficulty in the prediction of dilute nitride band gaps, however, a control is indicated. The SQS cells of different sizes yield a range of band gaps that are generally close to one another for a given concentration. For the lower concentrations of 3.7% and 7.4% N, the tested SQS cells agree well with the reference and clearly outperform the  $3^3$  supercells. This is especially noteworthy for the SQS-54 of the same size. For 7.4% N in particular, the agreement to the reference is remarkable for the SQS-54 (+0.02 eV) and the SQS-216 (+0.01 eV). For 11.1% N the picture changes somewhat, as the SQS cells strongly underestimate the band gap compared to the reference, yielding only slightly higher band gaps than the  $3^3$  supercells. This holds for all tested SQS cells, thus increasing the size does not mitigate this effect.

Based on the observations described above, it appears that the unavoidable periodicity prevents the strain field and the N-centered CB states from decaying sufficiently for high concentrations such as 11.1% N even for larger SQS cells. In particular, the SQS cells tend to have one very short axis, which reduces the distance between translational images and is probably the cause for the underestimation of band gaps in the SQS approach. The  $6^3$  supercells on the other hand seems to fulfill this requirement even for larger concentrations. However, for  $N^3$  supercells, scattering of band gap values is inevitable, making sampling a necessity. Thus, for smaller concentrations of N in Ga(NAs), SQS cells remain a viable, very efficient alternative, especially since small SQS cells are sufficient in the cases where the SQS approach is applicable.

Figure 3 shows band gaps we calculated using the  $6^3$  supercell and the band gap decrease as predicted by the CBAC model. For the three lower concentrations (1.9%, 3.4%, and 5.6%), four arrangements have been averaged, three for 7.4%

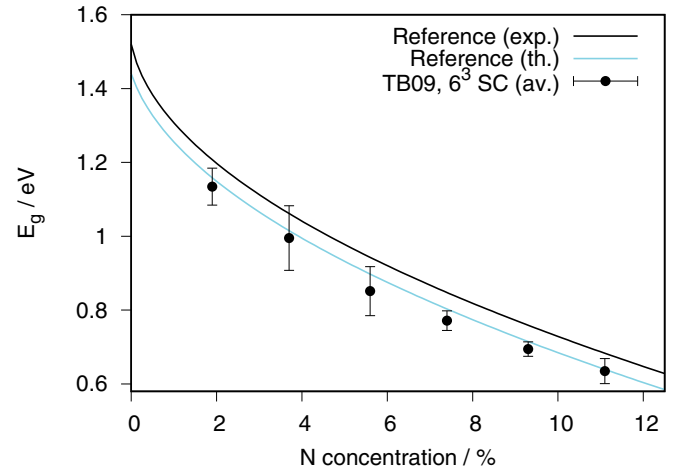


FIG. 3. Band gaps of Ga(NAs) for a  $6^3$  supercell averaged over four arrangements each for the three concentrations up to 5.6% N, three arrangements each for 7.4 and 9.3% N and two for 11.1%. The references are based on the CBAC model parameters as given by Ref. [45] with the experimentally derived band gap (exp.) and with the TB09 band gap (th.) of GaAs (see Table I).

and 9.3% and two for 11.1%. Since different local motifs are more likely to be repeated for higher concentrations, the scattering of values tends to decrease (indicated as error bars in Fig. 3). Using the experimental band gap for GaAs  $E_g = 1.52$  eV and the CBAC model parameters from Ref. [45], the predicted band gaps are overall larger than our calculated ones. However, since our supercell calculations are based on the TB09 functional, which yielded a band gap of  $E_g = 1.44$  eV (see Table I), this theoretical (th.) value should be used with the CBAC model in order to allow for comparability. Indeed, an excellent agreement between CBAC (th.) and the supercell band gaps is found in Fig. 3.

It can be concluded that a  $6^3$  supercell is indeed large enough to counteract the artificial interaction with periodic images that plagues smaller supercells, while SQS of smaller size can be used for computing band gaps at lower N concentrations, yet they seem too small at higher concentration. The band gap for a specific cell can depend strongly on its particular configuration, which leads to an appreciable scattering up to  $\pm 100$  meV in extreme cases. Small concentrations seem to be more susceptible to this, since they have a less even distribution of N atoms. The averaged band gaps, however, fall into a few tenths of an eV from the (theoretical) reference.

## F. Band gap range for N-atom clustering

In order to cast some light on the configurational dependence of the band gap within the approach described in this work, we computed the band gaps of various nonrandom arrangements of four N atoms in a  $6^3$  supercell (1.9% N). In particular, we used arrangements of two N ( $N_2$ ) and three ( $N_3$ ) atoms on neighboring positions. In the former case, two such clusters were present in order to exclude the influence of further structural motifs, and the clusters were either on the same line (paired) or on different lines (unpaired) along the crystallographic directions  $\{100\}$ ,  $\{110\}$ , and  $\{111\}$ ; in the

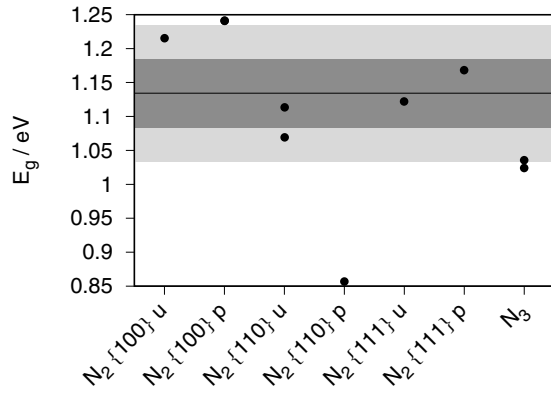


FIG. 4. Band gaps of nonrandom clustered configurations of a  $\text{Ga}_{216}(\text{N}_4\text{As}_{212})$  supercell. The labels identify the cluster size, crystallographic direction, and whether two clusters are paired (p) or unpaired (u). The black line marks the average of the random configurations, the dark and light shaded areas the standard deviation of those and twice that value, respectively.

latter case, the fourth atom was placed at some distance from the  $\text{N}_3$  cluster, the atoms of which are connected to one Ga atom. The  $\text{N}_2$  configurations are referred to as clusters due to them being placed on adjacent lattice positions, despite not necessarily sharing a common Ga atom. The band gaps from these calculations are summarized in Fig. 4.

As can be seen, the band gaps scatter significantly over different types of clusters and to a lesser extent over different realizations of a particular motif, e.g., the two data points for  $\text{N}_3$ . The band gaps fall in the vicinity of the average value for random distributions, with the exception of the paired  $\{110\}$  clusters. These form a periodic, channel-like state which greatly reduces the band gap, similar to the artificial periodicity induced by smaller cells.  $\text{N}$  atoms sharing a Ga atom, such as for  $\text{N}_2$  clusters along  $\{110\}$  and  $\text{N}_3$  clusters, have a reduced band gap compared to more isolated arrangements in accordance with the observed extension of  $\text{N}$  states along the  $\{110\}$  chains.

Ignoring the outlier of the paired  $\{110\}$  chain, the band gaps scatter about twice as much as the standard deviation of the random configurations, showing the strong effect that clustering can have due to the formation of cluster states between interacting  $\text{N}$  atoms. This should be taken into consideration when modeling materials grown under nonequilibrium conditions where clustering might occur depending on the actual growth process.

### G. Effective band structure of $\text{Ga}(\text{NAs})$

In order to predict optical properties from *ab initio* calculations, it is necessary to go beyond the computation of band gaps alone. To explore the possibility for the system at hand, a part of the band structure along the  $\Delta$  and  $\Lambda$  high symmetry axes in the immediate vicinity of the  $\Gamma$  point was computed and unfolded using a custom unfolding routine for the single arrangement of  $\text{Ga}_{216}\text{N}_8\text{As}_{208}$  already used above. The effective band structure (EBS) is shown and compared with a 10-band CBAC  $\mathbf{k} \cdot \mathbf{p}$ -band structure [6,45,47,48] in Fig. 5. Despite the simplistic CBAC model with a single

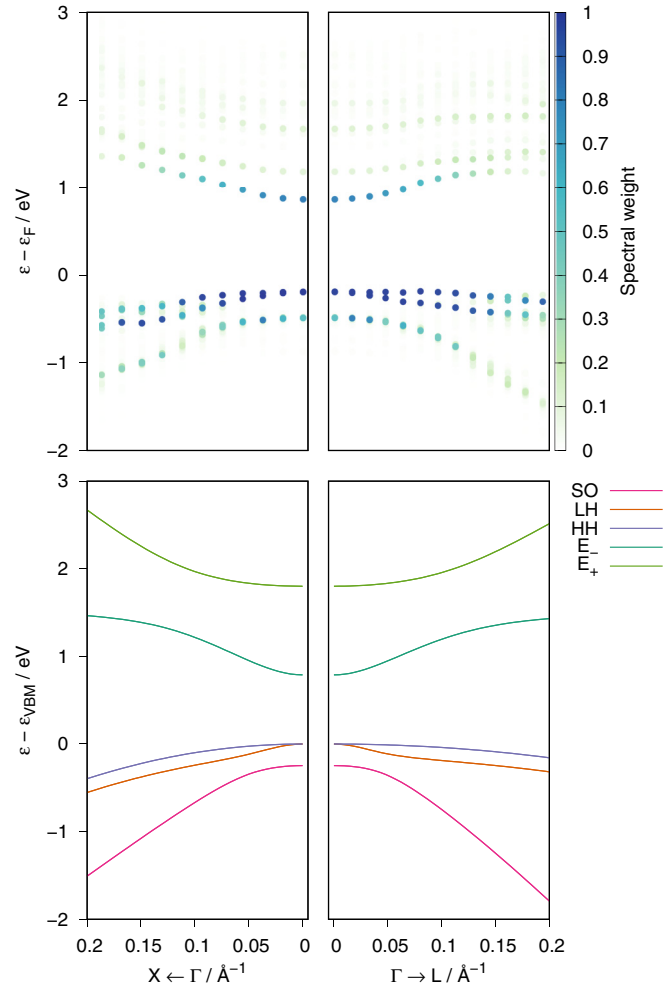


FIG. 5. Effective band structure of a  $6^3$  supercell of  $\text{Ga}(\text{N}_{0.037}\text{As}_{0.963})$  along  $\Delta$  and  $\Lambda$  high symmetry axes (top row) contrasted to a  $\mathbf{k} \cdot \mathbf{p}$ -band structure obtained from a 10 band conduction band anticrossing Hamiltonian (bottom row).

nitrogen level, the overall agreement between both approaches is rather good, especially for the valence bands. The two conduction bands described by the CBAC model can be identified in the DFT derived EBS, however, one additional band with a spectral weight of roughly 0.2 and several other bands with lower spectral weight occur in the EBS. The  $E_+$  band of the  $\mathbf{k} \cdot \mathbf{p}$ -band structure can be considered as an average of the higher bands in this context. However, the additional band right above the lowest conduction band is not accounted for by the CBAC model. It is noticeable that these weak higher bands have a very small dispersion compared to other bands and especially to the  $E_+$  band in the  $\mathbf{k} \cdot \mathbf{p}$  model. While we did not set out to consider cluster states specifically, more localized states on the  $\text{N}$  atoms are expected to manifest on this manner, as can be seen in other studies [46,49,50]. Since the  $E_-$  band has a higher spectral weight and is lower in energy, it is the most relevant for the computation of optical properties. Thus, this issue does not invalidate the CBAC- $\mathbf{k} \cdot \mathbf{p}$  model as a starting point for this purpose. Nevertheless, the existence of an intermediate band may be relevant for higher excitations.

#### IV. DISCUSSION AND CONCLUSIONS

In summary, we revisited the long standing issue of *ab initio* calculations of the electronic structure of dilute nitrides by combining a density functional producing quantitative band gaps (TB09) with a converged supercell approach. Our computed band gaps are in excellent agreement with the established CBAC model for the Ga(NAs) system. The required supercell size is determined by the extension of the distortion field introduced by the N atom in the GaAs lattice and its electronic states. Even with a functional that produces good band gaps, the supercell size must be large enough to avoid spurious interactions of the N atom with its translational image, which manifests itself in the strong overestimation of relaxation effects on the band gap. Comparison with the SQS approach showed that this design principle allows us to reach superior results compared to simple supercells of the same size also for the Ga(NAs) material system. At higher N concentrations, however, simple supercells of sufficient size allow for an easy and fast access to the electronic properties of dilute nitrides making it possible for us to systematically study the effect of N atom arrangements.

DFT calculations in combination with the empirical pseudopotential method (EPM) developed by Zunger *et al.* makes it possible to use significantly larger unit cells than our approach and thus allows for the modeling of stronger disorder [11,12,15,51,52]. However, the DFT/EPM approach requires and relies on empirical input for the pseudopotential to produce accurate band gaps, while our approach uses a functional that is built to compute accurate electronic structures with any suitable pseudopotential, allowing for a more uniform approach (e.g., the structural relaxation can be performed on a DFT level rather than applying force fields).

Comparing to GW [9] and even hybrid DFT [14] calculations, the TB09 functional offers comparable or better accuracy, respectively, for smaller computational cost, which makes it possible to use larger simulation cells than with those approaches. Apart from the numerical accuracy regarding band

gaps, other specifics of dilute Ga(NAs) are reproduced as well by our approach. As shown in Secs. III B and III C, the known interplay between the lattice mismatch of GaAs and GaN and the structural relaxation in Ga(NAs) [15] and the related extension of N-centered conduction band states along the {110} zigzag lines are well reproduced by the TB09 functional. The latter are known to be connected to the strong bowing [15,16].

Compared to tight-binding calculations, the approach described here is again limited to smaller model systems, but less reliant on empirical input. These studies showed additional (cluster) states between the  $E_+$  and the  $E_-$  band of the CBAC model [46,49,50]. As demonstrated in the previous section, we see similar states with low dispersion in the effective band structure, showing that this feature is captured by the combination of the TB09 functional and relatively compact supercells.

Altogether, we strongly believe that the approach described in this paper offers an attractive alternative for the electronic structure modeling in dilute nitrides. The use of the TB09 functional fixes the difficulty of other density functionals regarding the computation of band gaps. At the same time, our supercells can be kept relatively small compared to more empirical, computationally cheaper approaches such as the EPM or tight binding, alleviating the dependence on experimentally derived data to some degree. On the other hand, this relatively small supercell size makes the inclusion of several structural motifs at once more difficult and necessitates sampling over different configurations. Given the good reproduction of dilute nitride band gaps and the appearance of the expected N-cluster states between the  $E_-$  and  $E_+$  bands, we are convinced that our approach is promising for predictive computations.

#### ACKNOWLEDGMENTS

This work was supported by the German Research Foundation (DFG) in the framework of the Research Training Group “Functionalization of Semiconductors” (GRK 1782). The authors thank the HRZ Marburg, CSC-LOEWE Frankfurt, and HLR Stuttgart for providing computational resources.

- 
- [1] M. Kondow, K. Uomi, A. Niwa, T. Kitatani, S. Watahiki, and Y. Yazawa, *Jpn. J. Appl. Phys.* **35**, 1273 (1996).
  - [2] B. Kunert, S. Reinhard, J. Koch, M. Lampalzer, K. Volz, and W. Stolz, *Phys. Status Solidi C* **3**, 614 (2006).
  - [3] M. Weyers, M. Sato, and H. Ando, *Jpn. J. Appl. Phys.* **31**, L853 (1992).
  - [4] M. Kondow, K. Uomi, K. Hosomi, and T. Mozume, *Jpn. J. Appl. Phys.* **33**, L1056 (1994).
  - [5] K. Uesugi, N. Morooka, and I. Suemune, *Appl. Phys. Lett.* **74**, 1254 (1999).
  - [6] W. Shan, W. Walukiewicz, J. Ager, E. Haller, J. Geisz, D. Friedman, J. Olson, and S. Kurtz, *Phys. Rev. Lett.* **82**, 1221 (1999).
  - [7] L. C. Bannow, O. Rubel, S. C. Badescu, P. Rosenow, J. Hader, J. V. Moloney, R. Tonner, and S. W. Koch, *Phys. Rev. B* **93**, 205202 (2016).
  - [8] D. G. Thomas and J. J. Hopfield, *Phys. Rev.* **150**, 680 (1966).
  - [9] A. Rubio and M. L. Cohen, *Phys. Rev. B* **51**, 4343 (1995).
  - [10] S.-H. Wei and A. Zunger, *Phys. Rev. Lett.* **76**, 664 (1996).
  - [11] L. Bellaiche, S.-H. Wei, and A. Zunger, *Phys. Rev. B* **54**, 17568 (1996).
  - [12] L. Bellaiche, S. Wei, and A. Zunger, *Appl. Phys. Lett.* **70**, 3558 (1997).
  - [13] Y. Zhang, B. Fluegel, M. C. Hanna, A. Mascarenhas, L.-W. Wang, Y. J. Wang, and X. Wei, *Phys. Rev. B* **68**, 075210 (2003).
  - [14] V. Virkkala, V. Havu, F. Tuomisto, and M. J. Puska, *Phys. Rev. B* **85**, 085134 (2012).
  - [15] P. R. C. Kent and A. Zunger, *Phys. Rev. B* **64**, 115208 (2001).
  - [16] V. Virkkala, V. Havu, F. Tuomisto, and M. J. Puska, *Phys. Rev. B* **88**, 035204 (2013).
  - [17] A. Zunger, *Phys. Status Solidi B* **216**, 117 (1999).
  - [18] J. P. Perdew and Y. Wang, *Phys. Rev. B* **45**, 13244 (1992).
  - [19] J. P. Perdew, *Int. J. Quantum Chem.* **28**, 497 (1985).
  - [20] J. P. Perdew, K. Burke, and M. Ernzerhof, *Phys. Rev. Lett.* **77**, 3865 (1996).

- [21] A. V. Krukau, O. A. Vydrov, A. F. Izmaylov, and G. E. Scuseria, *J. Chem. Phys.* **125**, 224106 (2006).
- [22] J. E. Moussa, P. A. Schultz, and J. R. Chelikowsky, *J. Chem. Phys.* **136**, 204117 (2012).
- [23] A. Zunger, S.-H. Wei, L. G. Ferreira, and J. E. Bernard, *Phys. Rev. Lett.* **65**, 353 (1990).
- [24] F. Tran and P. Blaha, *Phys. Rev. Lett.* **102**, 226401 (2009).
- [25] Y.-S. Kim, M. Marsman, G. Kresse, F. Tran, and P. Blaha, *Phys. Rev. B* **82**, 205212 (2010).
- [26] H. Jiang, *J. Chem. Phys.* **138**, 134115 (2013).
- [27] G. Kresse and J. Hafner, *Phys. Rev. B* **47**, 558 (1993).
- [28] G. Kresse and J. Hafner, *Phys. Rev. B* **49**, 14251 (1994).
- [29] G. Kresse and J. Furthmüller, *Comput. Mater. Sci.* **6**, 15 (1996).
- [30] G. Kresse and J. Furthmüller, *Phys. Rev. B* **54**, 11169 (1996).
- [31] P. E. Blöchl, *Phys. Rev. B* **50**, 17953 (1994).
- [32] G. Kresse and D. Joubert, *Phys. Rev. B* **59**, 1758 (1999).
- [33] H. J. Monkhorst and J. D. Pack, *Phys. Rev. B* **13**, 5188 (1976).
- [34] S. Grimme, J. Antony, S. Ehrlich, and H. Krieg, *J. Chem. Phys.* **132**, 154104 (2010).
- [35] S. Grimme, S. Ehrlich, and L. Goerigk, *J. Comput. Chem.* **32**, 1456 (2011).
- [36] P. Vinet, J. Ferrante, J. R. Smith, and J. H. Rose, *J. Phys. C* **19**, L467 (1986).
- [37] J. P. Perdew, M. Ernzerhof, and K. Burke, *J. Chem. Phys.* **105**, 9982 (1996).
- [38] L. G. Ferreira, M. Marques, and L. K. Teles, *Phys. Rev. B* **78**, 125116 (2008).
- [39] L. G. Ferreira, M. Marques, and L. K. Teles, *AIP Adv.* **1**, 032119 (2011).
- [40] ATOM, <http://www.gmsn.ita.br/downloads/instructions.tar.bz2>.
- [41] V. Popescu and A. Zunger, *Phys. Rev. B* **85**, 085201 (2012).
- [42] A. Van De Walle, P. Tiwary, M. De Jong, D. L. Olmsted, M. Asta, A. Dick, D. Shin, Y. Wang, L. Q. Chen, and Z. K. Liu, *CALPHAD: Comput. Coupling Phase Diagrams Thermochem.* **42**, 13 (2013).
- [43] See Supplemental Material at <http://link.aps.org/supplemental/10.1103/PhysRevB.97.075201> for cell specific band gaps and structural data of optimized cells.
- [44] I. Vurgaftman, J. R. Meyer, and L. R. Ram-Mohan, *J. Appl. Phys.* **89**, 5815 (2001).
- [45] I. Vurgaftman and J. R. Meyer, *J. Appl. Phys.* **94**, 3675 (2003).
- [46] E. P. O'Reilly, A. Lindsay, and S. Fahy, *J. Phys.: Condens. Matter* **16**, S3257 (2004).
- [47] A. Lindsay and E. P. O'Reilly, *Solid State Commun.* **112**, 443 (1999).
- [48] E. P. O'Reilly, A. Lindsay, S. Tomi, and M. Kamal-Saadi, *Semicond. Sci. Technol.* **17**, 870 (2002).
- [49] A. Lindsay and E. P. O'Reilly, *Phys. Rev. Lett.* **93**, 196402 (2004).
- [50] F. Masia, G. Pettinari, A. Polimeni, M. Felici, A. Miriametro, M. Capizzi, A. Lindsay, S. B. Healy, E. P. O'Reilly, A. Cristofoli, G. Bais, M. Piccin, S. Rubini, F. Martelli, A. Franciosi, P. J. Klar, K. Volz, and W. Stolz, *Phys. Rev. B* **73**, 073201 (2006).
- [51] P. R. C. Kent and A. Zunger, *Phys. Rev. Lett.* **86**, 2613 (2001).
- [52] P. R. C. Kent, L. Bellaiche, and A. Zunger, *Semicond. Sci. Technol.* **17**, 851 (2002).